A Magnetic Field Code for Handling General Current Carrying Conductors in Three Dimensions

T.F. Yang

May 1975

UWFDM-123

FUSION TECHNOLOGY INSTITUTE

UNIVERSITY OF WISCONSIN

MADISON WISCONSIN

A Magnetic Field Code for Handling General Current Carrying Conductors in Three Dimensions

T.F. Yang

Fusion Technology Institute
University of Wisconsin
1500 Engineering Drive
Madison, WI 53706

http://fti.neep.wisc.edu

May 1975

UWFDM-123

A Magnetic Field Code for Handling General Current Carrying Conductors in Three Dimensions - MAFCO-W

by

T. F. Yang

UWFDM-123

Fusion Technology Program
Nuclear Engineering Department
University of Wisconsin
Madison, Wisconsin 53706

A MAGNETIC FIELD CODE FOR HANDLING GENERAL CURRENT CARRYING CONDUCTORS IN THREE DIMENSIONS - MAFCO-W

T. F. Yang Nuclear Engineering Department, The University of Wisconsin, Madison, Wisconsin, U.S.A.

ABSTRACT

A computer code MAFCO-W has been written for calculating magnetic fields of finite size conductors of general configuration which can be approximated by arc segments or straight segments of rectangular cross section. The magnetic field components were obtained by integrating the Biot-Savat's law over the volume of the conductor. Their mathematic expressions were first reduced to single integration analytically and then integrated numerically. The magnetic fields for the conceptual Tokamak fusion reactors UWMAK-I [1,2] and II [3] were calculated and analyzed.

1. INTRODUCTION

A general magnetic field code MAFCO-W which is a modified and extended version of the original MAFCO [4] has been developed. These codes are used to calculate the magnetic fields produced by a distribution of current in three dimensions of any configuration. The major difference between MAFCO-W and MAFCO is that MAFCO-W can calculate accurately, and with high efficiency, the magnetic field inside as well as outside a conductor of rectangular cross section carrying uniformly distributed current. The capability of calculating the field in all space, particularly within the conductor, is required for superconducting magnet design. MAFCO handles only the case of separated filament windings so that a finite conductor must be approximated by a large number of filaments. The MAFCO calculation could therefore become very expensive and lead to inaccurate results within the conductor due to singularities of the filaments.

MAFCO-W approximates a conductor of general configuration by arc and straight segments. The field is calculated by integrating the Biot-Savat law over the volume of the arc or straight segments. Three dimensional integrations are involved. The expressions for the field components have been reduced to a single integration analytically. The final integration is carried out numerically by employing the Gaussian Quadrature technique. Therefore MAFCO-W is able to calculate the field both outside and inside a conductor with much greater accuracy and efficiency, especially when a large cross section conductor is involved.

The field structures calculated using MAFCO-W for the D-shaped toroidal magnets of the conceptual designs of Tokamak fusion reactors UWMAK-I [1,2] and II [3] will be presented and discussed.

II. THEORY

II-1. THE MAGNETIC FIELD FROM A CIRCULAR ARC SEGMENT AND RING

As is shown by Figure 1, the magnetic field at the point $p(R_p,\theta_p,Z_p)$ from a source element at the the point (ρ,ϕ,Z) is given by the Biot-Savart law:

$$d\vec{B}_p = j\,\vec{d\ell} \times \vec{R}\, d\rho\, dZ/10\, R^3 \qquad (1)$$

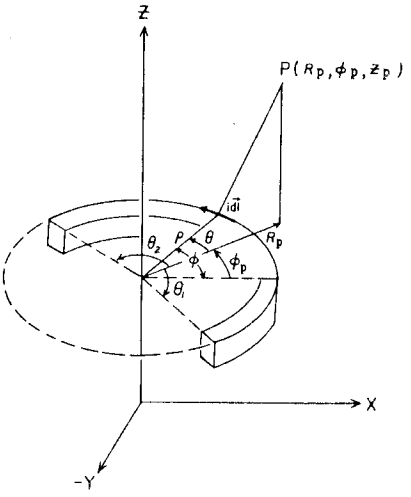

Figure 1 - Arc Segment Coordinates

where j is the current density in amp/cm^2 and $\vec{R}$ is the position vector from $\vec{d\ell}$ to p which is

$$R^2 = R_p^2 - 2R_p\,\rho\cos(\phi_p-\phi) + \rho^2 + (Z_p-Z)^2 \qquad (2)$$

Letting $\theta = \phi-\phi_p$

$$d\ell = \hat{R}_p \cdot \rho d\theta\sin\theta + R_p\hat{\phi}_p \cdot \rho d\theta\cos\theta + \hat{Z}_p \cdot 0, \qquad (3)$$

and $\vec{R} = \hat{R}_p \cdot (R_p-\rho\cos\theta) + R_p\hat{\phi}(\rho\sin\theta) + \hat{Z}(Z_p-Z).$

The vector product of $\vec{R}$ and $\vec{d\ell}$ is

$$\vec{R}\times\vec{d\ell} = \hat{R}_p[\rho(Z_p-Z)\cos\theta d\theta] + \hat{\phi}_p(Z_p-Z)\rho\sin\theta\, d\theta + \hat{Z}(\rho^2 - R_p\,\rho\cos\theta)d\theta. \qquad (4)$$

Thus the components of $d\vec{B}_p$ are

$$dB_{R_p} = \frac{j(Z_p-Z)\rho\cos\theta\, dZ\, d\rho\, d\theta}{10[\rho^2-2\rho\,R_p\cos\theta + R_p^2+(Z_p-Z)^2]^{3/2}}, \qquad (5)$$

$$dB_{\phi_p} = \frac{j(Z_p-Z)\rho\sin\theta\, dZ\, d\rho\, d\theta}{10[\rho^2-2\rho\,R_p\cos\theta + R_p^2+(Z_p-Z)^2]^{3/2}}, \qquad (6)$$

and $$dB_{z_p} = \frac{j(\rho^2-\rho R_p\cos\theta)dZ\ d\rho\ d\theta}{10[\rho^2-2\rho\ R_p\cos\theta+R_p^2+(Z_p-Z)^2]^{3/2}}\ . \quad (7)$$

In the following discussions, the integration limits are from θ_1 to θ_2, Z_1 to Z_2 and ρ_1 to ρ_2, unless otherwise specified, for a circular arc of rectangular cross section. B_θ can be obtained exactly if we integrate equation (6) over θ and Z successively, thus

$$B_{\phi_p} = \frac{j}{10}\int d\rho\int dZ\ \frac{(Zp-Z)dZ}{R_p[\rho^2-2R_p\rho\cos\theta+R_p^2+(Z_p-Z)^2]^{3/2}} + C,$$

$$= -\frac{j}{10}\int\frac{1}{R}\ [\rho^2-2R_p\rho\cos\theta+R_p^2+(Z_p-Z)^2]^{1/2}d\rho + C. \quad (8)$$

This can be rewritten as

$$B_{\phi_p} = -\frac{j}{10\ R_p}\int[(\rho-R_p\cos\theta)^2+R_p^2\sin^2\theta+(Z_p-Z)^2]^{1/2}d\rho+C, \quad (9)$$

integrating we obtain

$$B_{\phi_p} = -\frac{j}{20\ R_p}\{(\rho-R_p\cos\theta)R_p+[R_p^2+\sin^2\theta+(Z_p-Z)^2]\cdot \log[(\rho-R_p\cos\theta)R]\} + C, \quad (10)$$

where R is given by equation (2). For the components B_ρ and B_Z the integrations over Z and ρ can be carried out. Integrating equations (6) and (7) following T. H. Boyer et al.[5] yields the following results:

$$B_{R_p} = \frac{j}{10}\int d\theta\cos\theta\{R+R_p\cos\theta\log(\rho-R_p\cos\theta+R)\}+C, \quad (11)$$

and $$B_{Z_p} = \frac{j}{10}\int d\theta(Z-Z_p)\{\log(\rho-R_p\cos\theta+R)+\frac{R_p\cos\theta}{2|Z_p-Z|}\cdot\log\frac{R-|Z_p-Z|}{R+|Z_p-Z|} - \frac{R_p|\sin\theta|}{|Z_p-Z|}\tan^{-1}\left[\frac{(\rho-R_p\cos\theta)|Z_p-Z|}{R_p|\sin\theta|R}\right]\} + C. \quad (12)$$

For the field point at the Z-axis, B_ρ, B_ϕ and B_Z become

$$B_{R_p} = \frac{j}{10}(Z-Z_p)\log(\rho+\sqrt{\rho^2+(Z_p-Z)^2}) + C, \quad (13)$$

$$B_{\phi_p} = \frac{j}{10\ R_p}\cos\theta[\rho^2 + (Z_p-Z)^2]^{1/2} + C, \quad (14)$$

and $$B_{Z_p} = \frac{j}{10}(Z-Z_p)\log\left\{\frac{R+[R^2+(Z_p-Z)^2]^{1/2}}{R+[R^2+(Z_p-Z)^2]^{1/2}}\right\} + C. \quad (15)$$

In the case of circular ring of rectangular cross section, the expression for B_ρ, B_ϕ and B_Z are the same as equations (8), (9), and (10) and (11), except that the integration limits over θ are from 0 to 2π. Due to the symmetry property of B_ρ and B_Z, we can just integrate them from 0 to π and multiply the results by 2. It follows that B_ϕ is zero everywhere and B_ρ is zero on the z-axis.

II-2. FIELD FROM A STRAIGHT SEGMENT OF RECTANGULAR CROSS SECTION

If we transform an arbitrarily oriented current carrying straight segment of conductor to a coordinate such that the current flows in the Z-direction as shown by Figure 2, then the field at the point $p(X_p,Y_p,Z_p)$ due to a current element $\vec{dz}$ at the source point (x,y,z) is

$$\vec{dB} = \frac{j\ dx\ dy}{10\ R^3}\ (\vec{dz}\times\vec{R}),$$

$$= \frac{j\ \rho}{10\ R^3}\ \hat{z}\times\hat{R}\ dx\ dy\ dz, \quad (16)$$

where

$$\rho = \sqrt{(Z_p-x)^2 + (Y_p-y)^2} \quad (17)$$

and

$$R = \sqrt{(X_p-x)^2 + (Y_p-Y)^2 + (Z_p-Z)^2} \quad (18)$$

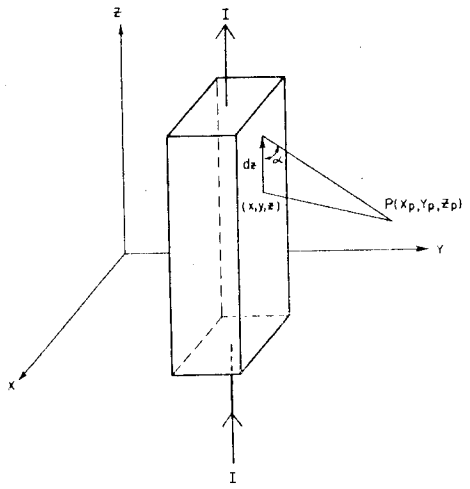

Figure 2 - Straight Segment Coordinates

The x and y components of $\vec{dB}$ are

$$dB_{x_p} = -\frac{j}{10}\ \frac{Y_p - Y}{R^3}\ dx\ dy\ dZ, \quad (19)$$

and $$dB_{y_p} = +\frac{j}{10}\ \frac{X_p - X}{R^3}\ dx\ dy\ dZ. \quad (20)$$

After carrying out the integration of Z in equation (16)

$$B_{x_p} = \iint -\frac{j}{10}\frac{(Y_p-Y)(Z_p-Z)dx\,dy}{[(X_p-X)^2+(Y_p-Y)^2]}$$

$$\cdot[(X_p-X)^2+(Y_p-Y)^2+(Z_p-Z)^2]^{-2} + C. \qquad (21)$$

Making the substitution $t^2=(X_p-X)^2+(Y_p-Y)^2+(Z_p-Z)^2$ we can integrate out Y and obtain

$$B_{x_p} = -\frac{j}{20}\int dx\,\frac{(Z_p-Z)}{|Z_p-Z|}\log\frac{R-|Z_p-Z|}{R+|Z_p-Z|} + C. \qquad (22)$$

Similarly, the y-component of B is

$$B_{y_p} = -\frac{j}{10}\int dy\,\frac{(Z_p-Z)}{|Z_p-Z|}\log\frac{R-|Z_p-Z|}{R+|Z_p-Z|} + C. \qquad (23)$$

Equations (19) and (20) contain the same integral which is integrated numerically.

III. CONSIDERATIONS FOR NUMERICAL INTEGRATIONS

The integrations in equations (11), (12), (22) and (23) were carried out numerically using a Gaussian Quadrature method. For reasons of economy, the order of the Gaussian integration was varied proportionally with angular length of the arc segment. The lowest order used is 4 and the highest order is 35. In most cases, order 20 was found to be sufficient to obtain an accuracy as good as 10^{-5} for a 180° arc segment if the integrands are well behaved functions which is the case when the field is being calculated on the outside of the conductor. However, when the field is being calculated on the inside of the conductor, the integrands would have singularity, then the integrations are broken into parts and the higher order Gaussian integration is used.

In order to improve the accuracy, or for certain special cases, to obtain reasonable results, expansions of the integrands have to be made as follows

(1) If $2\rho R_p(1-\cos\theta) \ll (\rho-R_p)^2$ and $(\rho-r)<0$, then we use the expression

$$(\rho-R_p\cos\theta)+(\rho^2-2\rho R_p\cos\theta+R_p^2)^{1/2}$$

$$\cong R_p(1-\cos\theta) + (\rho - R_p)\cdot f(x) \qquad (24)$$

in equation (11), where the function

$$f(x) = \frac{1}{2}(x - \frac{1}{2}x^2 + \frac{1}{8}x^3 - \frac{5}{64}x^4 + \ldots) \qquad (25)$$

and $x = 2\rho R_p(1-\cos\theta)/(\rho - R_p)^2$.

(2) If $\rho - 2\rho R_p\cos\theta + R_p^2 \ll (Z_p-Z)^2$, then the expression

$$(\rho^2-2\rho R_p\cos\theta)+R_p^2+(Z_p-Z)^2-|Z_p-Z| \cong |Z_p-Z|^2 f(x) \qquad (26)$$

is used in equation (12), where the function f(x) is defined as in case (1).

(3) If $|Z_p-Z| \gg [(X_p-X)^2+(Y_p-Y)^2]$, then the expression

$$[(X_p-X)^2 + (Y_p-Y)^2 + (Z_p-Z)^2]^{1/2} - |Z_p-Z|$$

$$\cong (Z_p - Z)f(u), \qquad (27)$$

is used in equations (19) and (20), where the function f(u) is defined as in case (1) but the argument u is

$$u = \frac{(X_p-X)^2 + (Y_p-Y)^2}{(Z_p - Z)^2}. \qquad (28)$$

IV. THE TOROIDAL MAGNETIC FIELD STRUCTURE OF THE CONCEPTUAL TOKAMAK FUSION REACTORS

The toroidal magnetic fields of UWMAK-I and UWMAK-II have been calculated using this code. The results are presented here. The magnetic field ripples produced by the finite number of coils were analyzed and the method for determining the number of coils needed to produce satisfactory axisymmetric toroidal field structures are discussed.

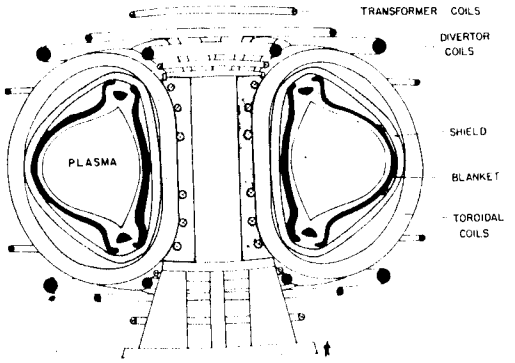

Figure 3 - Cross Section View of UWMAK-I Fusion Reactor

The cross section view of UWMAK-I fusion reactor is shown by Figure 3. For convenience of discussion, the coordinates of the toroidal system are shown in Figure 4 in which Z is the axis of axisymmetry, R is the major radius, r is the minor

radius, θ is the poloidal angle and ϕ is the toroidal angle. UWMAK-II contains 12 constant tension "D" shaped toroidal field coils spaced at equal toroidal angular intervals of 30°. The configuration of the upper half of each coils in shown in Figure 5. For the purposes of calculating the magnetic field each half of the coil is approximated

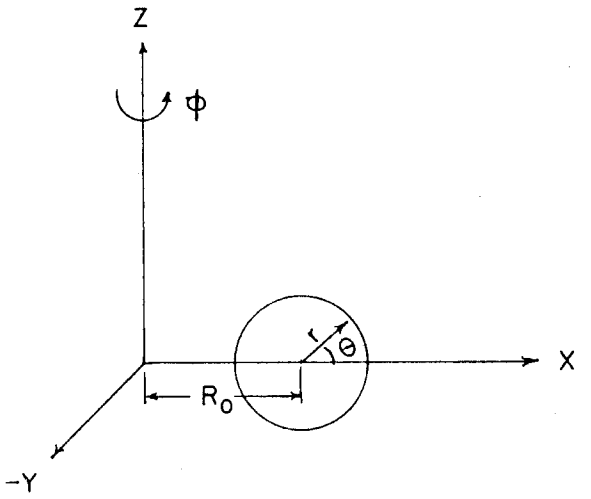

Figure 4 - Toroidal Coordinates

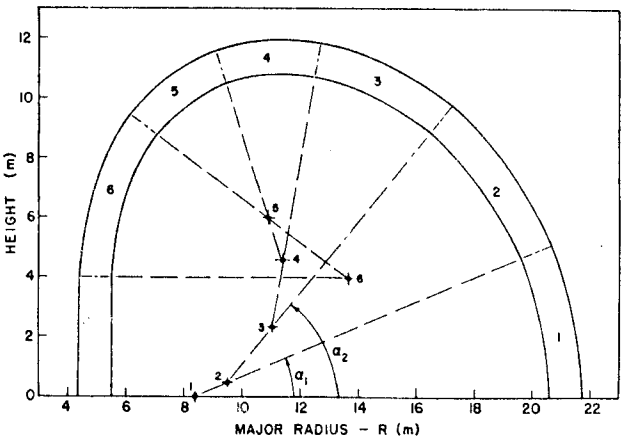

Figure 5 - Geometry of Toroidal Magnetic Field Coil

by 6 arc segments and one straight segment so as to give a close approximation to the coil shape. The dashed lines are the radii of curvatures and also define the poloidal angular limits of each arc segment. The calculated field pattern for the first quadrant at the midplane (x-y plane) is illustrated by some of the field lines shown in Figure 6. The field patterns in the other three quadrants are the same due to the periodicity of the coil arrangement. The cross sections of the toroidal field coils are indicated by the dashed rectangles. The plasma

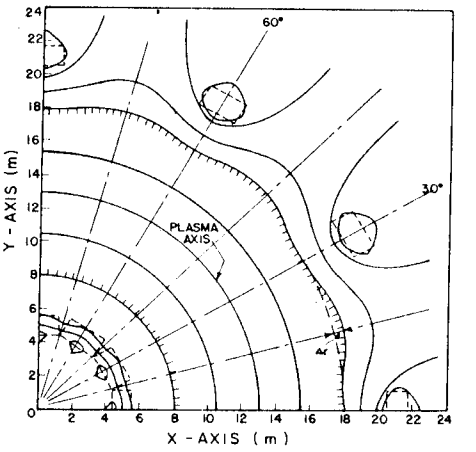

Figure 6 - Field Pattern on Midplane of Torus

occupies the space within the shaded field lines. The magnetic axis at the R_o = 13 meters and the minor radius is a = 5 meters. Figure 7 shows the variation of the amplitude of the field along the major radii at ϕ = o° and 15° on the midplane, where ϕ = 15° is the center of the gap between the first two adjacent coils and X = $(R-R_o)/a$ = r/a. Ideally,

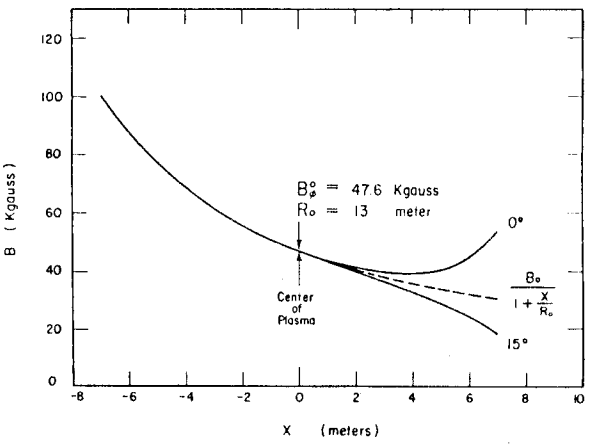

Figure 7 - Field Magnitude Along Minor Radius at Midplane

the toroidal field would have a 1/R dependence in the region of plasma if it would be perfectly axi-symmetric which is indicated by the solid curve to the left of center and dashed curve to the right of of the center. However, the actual field deviated from this dependence beyond the center as indicated by the o° curve which has a larger field and by 15° curve which has a smaller field. The variation of B_ϕ in the toroidal direction is indicated in Figure 8 which is a plot of the magnitude of B_ϕ along the field line on the outer edge of the plasma. This toroidal angular variation of the ripples as functions of the minor radius r and of the poloidal angle θ for UWMAK-I are shown by curves I in Figures 9 and 10 respectively. These curves can be fitted by a power function $(r/a)^n$ multiplied

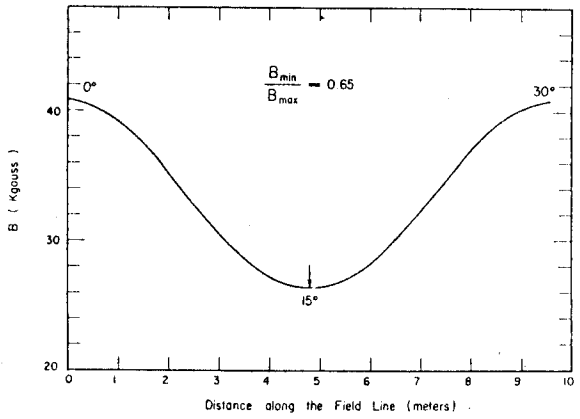

Figure 8 - Field Magnitude Along the Field Line at R = 18 m.

by a Gaussian function $\exp(\alpha\theta/\pi)^2$ taking n = 3 and α = 3. Therefore, the toroidal magnetic field can be modeled by the formulas

$$B_\phi(r,\theta,\phi) = \frac{R_o B_o}{R_o + r\cos\theta}\left[1+\epsilon_a\left(\frac{r}{a}\right)^n \exp\left(-\left(\frac{\alpha\theta}{\pi}\right)^2\right)\cdot\cos(Nq\theta+\phi_o)\right]. \quad (29)$$

where ϵ_a is the amplitude of the ripple at r = a. The charged particles in the plasma can be trapped in the localized magnetic wells of the ripples and drift toward the wall [6,7]. This means that 5.6% of the energetic alpha particles will not be magnetically confined but will strike the wall. This may cause additional wall damage and generation of impurities. To minimize this loss, we can increase the number of coils and/or extend the coils to larger major radius.

In order to obtain satisfactorily small field ripple with a minimum number of coils, we have calculated the variations of the ripples as functions of r and θ by extending the outer edge of the coils to R = 25 meters which is shown by Curves II in Figure 9 and 10. Curves III are the variations of

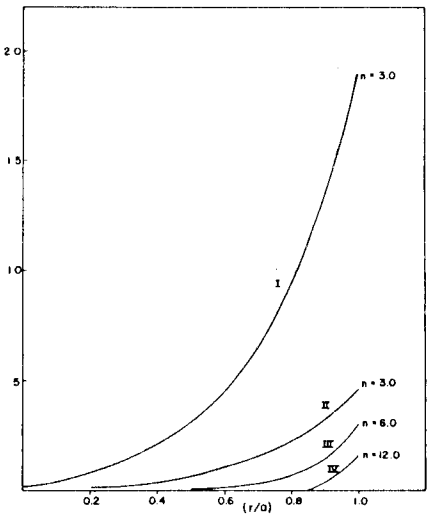

Figure 9 - Field Ripples in Percent as Functions of r. Curves I and II are for 12 coils and 12 extended coils respectively. Curves III and IV are for 24 coils and 24 extended coils, respectively.

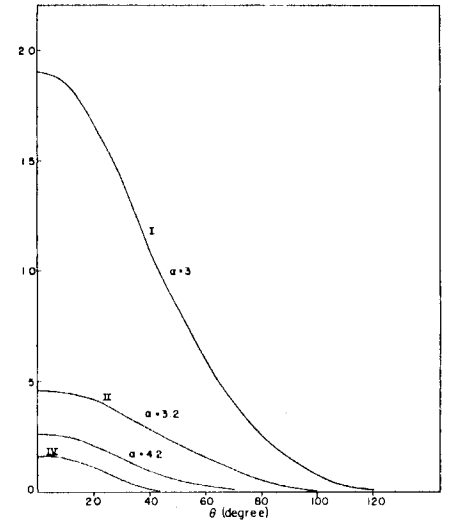

Figure 10 - Field Ripples in Percent as Functions of θ. Curves I and II are for 12 coils and 12 extended coils respectively. Curves III and IV are for 24 coils and 24 extended coils, respectively.

the ripples by doubling the coil number to 24. Curves IV are the same for 24 extended coils. These curves demonstrate that the ripples decrease rapidly

as the coil number and size increase. The alpha particle loss was found to be less than 0.1% for the design with 24 extended "D" coils. This is one of the major reasons for UWMAK-II to have 24 extended "D" coils. The toroidal magnetic field pattern is illustrated by some of the field lines in Figure 11. This figure shows that the plasma column is almost perfect axisummetric and the deviation at the outet edge is now only $\Delta r = 0.01$ meter. The amplitude of the field ripple is less than 0.01%.

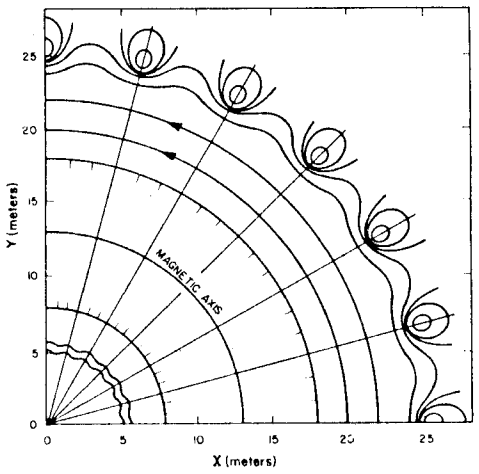

Figure 11 - Toroidal Magnetic Field Pattern for UWMAK-II

The magnetic fields inside the conductor for both UWMAK-I and II were also calculated. The contour of the constant |B| over the cross sections intersecting the midplane are shown in Figures 12 to 15. There are appreciable differences in the contours of |B| between the two designs. Further work is presently underway to calculate the magnetic forces and stresses on the magnet.

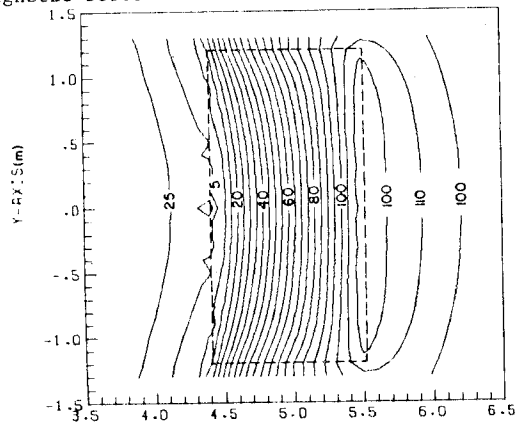

Fig. 12 Contour of magnitude |B| in kgauss plotted by computor. Dashed lines indicate the cross section of the coil intersected by the X-Y plane.

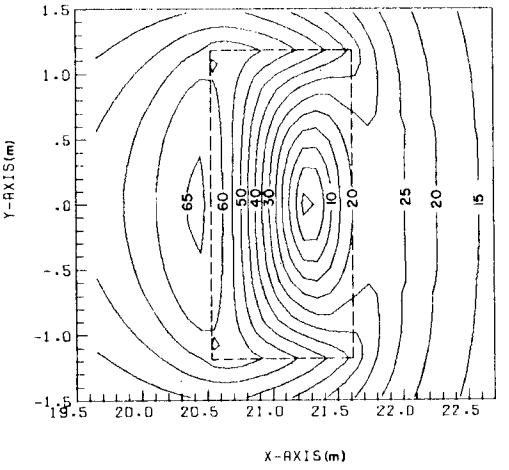

Figure 13 - Contour of magnitude |B| in kgauss plotted by computor. Dashed lines indicate the cross section of the coil intersected by the X-Y plane.

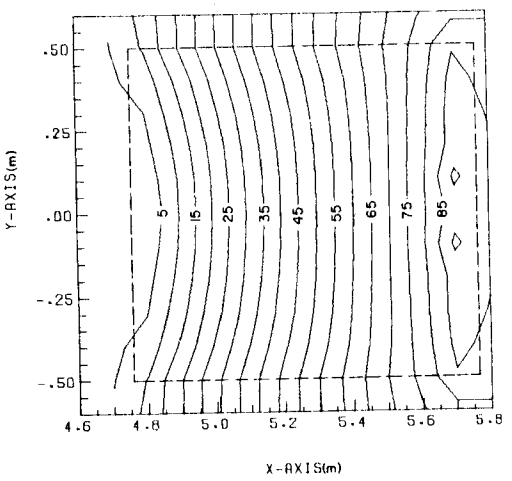

Figure 14 - Contour of magnitude |B| in kgauss plotted by computor. Dashed lines indicate the cross section of the coil intersected by the X-Y plane.

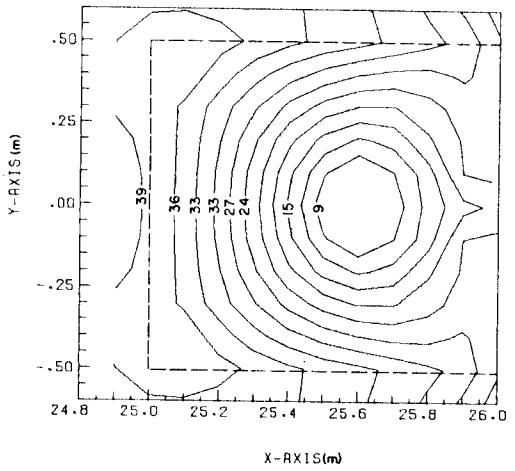

Figure 15 - Contour of magnitude |B| in kgauss plotted by computor. Dashed line indicates the cross section of the coil intersected by the X-Y plane.

V. ACKNOWLEDGEMENT

The author wishes to express his gratitude to Dr. J. Foote of Lawrence Radiation Laboratory in Livermore, California, for supplying the copy of MAFCO and his assistance in the conversion for running on UNIVAC-1110. The discussions with Prof. R. Boom of the University of Wisconsin and Prof. R. Christian of Purdue University were most valuable. This work is performed under the Wisconsin Fusion Reactor Technology Program supported by the USAEC and Wisconsin Electric Utility Research Foundation.

VI. REFERENCES

1. G. L. Kulcinski, R. W. Conn, Proc. 1st Nat'l. Top. Conf. on Cont. Nucl. Fusion (CONF-740402-P1, U.S.A.E.C., April 1974) Vol. 1, p. 38.

2. R. W. Conn and G. L. Kulcinski, ibid. Vol. 1, p. 56.

3. R. W. Conn et al., to be published in the Proc. 5th IAEA Conf. on Plasma Phys. and Cont. Nucl. Fus. Research, Tokyo, Japan (1974).

4. W. A. Perkins and J. C. Brown, "MAFCO - A Magnetic Field Code for Handling General Current Elements in Three Dimensions," LRL Rept. UCRL-7744-Rev. II.

5. T. H. Boyler and G. L. Droyles, Electromagnetic Field Code, Oak Ridge National Laboratory Rept., Rough Draft.

6. O. A. Anderson and H. P. Furth, Nuclear Fusion, 12, 207 (1972).

7. T. F. Yang and G. A. Emmert, Proc. 1st Top. Meeting on Cont. Nucl. Fusion (CONF-740402-P2, U.S.A.E.C., April 1974) Vol II, p. 400.

DISCUSSION. -

Müller G. : Could you please give some further comments on the calculation of fields inside the conductors ? This question is because the field becomes singular at the current lines.

Yang T. F. :

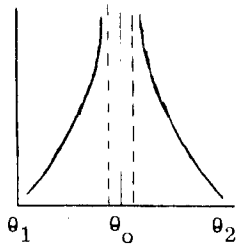

$$\int_{\theta_1}^{\theta_2} f = \int_{\theta_1}^{\theta_o} f + \int_{\theta_o}^{\theta_2} f$$

using gaussian quadrature we can make this integration. This can give enough accuracy as is demanded (1 %).

Preis H. : What is your definition of ripple equation ?

Yang T. F. :

$$\varepsilon = \frac{B_{max} - B_{min}}{2\,\frac{B_o}{1 + (\gamma/R)}}$$